Carbohydrate Polymers 87 (2012) 1670–1677

Contents lists available at SciVerse ScienceDirect

Carbohydrate Polymers

journal homepage: www.elsevier.com/locate/carbpol

Rheological properties of chitosan–tripolyphosphate complexes: From suspensions to microgels

Ji Li, Qingrong Huang*

Department of Food Science, Rutgers University, 65 Dudley Road, New Brunswick, NJ 08901-8520, USA

ARTICLE INFO

Article history:
Received 22 February 2011
Received in revised form 4 September 2011
Accepted 26 September 2011
Available online 1 October 2011

Keywords:
Chitosan (CS)
Sodium tripolyphosphate (TPP)
Rheological property
Particle packing

ABSTRACT

Complex fluids formed by crosslinking of chitosan (CS, 330 kDa) with sodium tripolyphosphate (TPP) have been studied by dynamic light scattering (DLS), atomic force microscopy (AFM), Fourier transform infrared spectroscopy (FTIR), and rheology. The effects of chitosan/TPP ratios, initial chitosan or TPP concentrations, and ultrasonication time on the chitosan–TPP complex formation have been investigated. It was found that the optimum condition for CS–TPP nanoparticle formation occurred at CS/TPP mass ratio of 3.75 and with 9 min sonication treatment (energy output 3.75 W/mL). At the same initial chitosan concentration, small particle sizes (i.e., particle size < 300 nm) resulted in the formation of CS–TPP nanoparticle suspensions, which showed a lower viscosity than pure chitosan solutions, and their viscosities increased as the CS–TPP nanoparticles sizes increased. Centrifugation of CS–TPP particles of larger particle sizes (i.e., 360–870 nm) at 11,000 × *g* caused the formation of CS–TPP microgels. Dynamic rheological studies indicated that both storage modulus (G') and loss modulus (G'') increased with particle sizes. During centrifugation processing, strong centrifugal force surmounted the electrostatic repulsion between CS–TPP particles and caused particles to stick with each other to form CS–TPP microgels. The water contents of microgels negligibly depended on particle size, suggesting that the free volumes of microgels were not affected by particle size, therefore supporting our pseudo-hard sphere assumption for CS–TPP nanoparticles.

1. Introduction

Chitosan (CS), the second most abundant biopolymer in nature next to cellulose, is one of the very few positively charged natural biopolymers existing in the world. It is derived from the exoskeleton of shrimps and other crustaceans, and has a linear structure composed of glucosamine unit and N-deacetylated glucosamine unit, also known as 2-amino-2-deoxy-(1 → 4)-β-D-glucopyranan. Chitosan has received broad attention from researchers of different backgrounds due to its unique structure and natural abundance (Yi et al., 2005). Previous literatures show that chitosan has been used to form complex coacervates (Espinosa-Andrews, Baez-Gonzalez, Cruz-Sosa, & Vernon-Carter, 2007), biocomposites (Luo et al., 2008), bio-carbon nanotubes (Zhang, Smith, & Gorski, 2004), and scaffolds for tissue engineering (Skotak, Leonov, Larsen, Noriega, & Subramanian, 2008). Other applications of chitosan include drug delivery systems, nanofibers, biosensors, and edible films (Han, Shan, Xue, & Cosnier, 2007; Zhang, Mardyani, Chan, & Kumacheva, 2006; Zhang, Su, Ramakrishna, & Lim, 2008). Among the above research areas, chitosan-based delivery system is one of the most important applications due to its biodegradability, biocompatibility, bioadhesion and non-toxicity (Janes, Calvo, & Alonso, 2001; Pillai & Panchagnula, 2001; Sogias, Williams, & Khutoryanskiy, 2008). Many investigations of chitosan-based delivery systems have been carried out previously. For example, Jang and Lee (2008) succeeded in improving the heat stability of L-ascorbic acid during processing by utilizing chitosan–TPP nanoparticles (Jang & Lee, 2008). Richardson, Kolbe, and Duncan (1999) conjugated chitosan to DNA backbone for protecting DNA from endonuclease degradation and promoting DNA's cell targeting (Richardson et al., 1999). Wu, Yang, Wang, Hu, and Fu (2005) applied CS–TPP nanoparticles for loading the drug ammonium glycyrrhizinate. The release profile of their CS–TPP nanoparticles followed the rule of first burst release and then steady release, suggesting that CS–TPP nanoparticle was a suitable oral delivery agent (Wu et al., 2005).

In order to meet different demands, distinct methods were used to produce chitosan nanoparticles. Chemical modification provides us with series of methods for producing stable chitosan nanoparticles. For instance, amphiphilic micellar structure of linolenic acid-modified chitosan could be immobilized with trypsin by using glutaraldehyde as the crosslinker, which greatly improved trypsin's thermal stability and enzymatic activity (Liu, Desai, Chen, & Park, 2005). Other researchers functionalized chitosan with multiple functional groups, such as octyl, sulfate and

* Corresponding author. Tel.: +1 732 932 7193; fax: +1 732 932 6776.
E-mail address: qhuang@aesop.rutgers.edu (Q. Huang).

0144-8617/$ – see front matter © 2011 Elsevier Ltd. All rights reserved.
doi:10.1016/j.carbpol.2011.09.074

polyethylene glycol monomethyl ether (mPEG) groups to target both polymeric micelle structure and brain-targeting function, and the resulted chitosan nanoparticles could improve the water solubility of hydrophobic drug paclitaxel by 4000 times (Yao, Zhang, Ping, and Yu, 2007). Very recently, a novel chitosan-based amphiphile, octanoylchitosan–polyethylene glycol monomethyl ether (acylChitoMPEG), has been synthesized using both hydrophobic octanoyl and hydrophilic polyethylene glycol monomethyl ether (MPEG) substitutions (Huang, Yu, Guo, & Huang, 2010). The synthesized acylChitoMPEG exhibited good solubility in either aqueous solution or common organic solvents such as ethanol, acetone, and $CHCl_3$. Cytotoxicity results showed that acylChitoMPEG exhibited negligible cytotoxicity even at the concentration as high as 1 mg/mL (Huang et al., 2010).

In addition to chemical synthesis, physical methods were also used to create chitosan complexes or nanoparticles with milder processing conditions. Since chitosan has hydroxyl and amino groups on the backbone, chitosan can interact with other negatively charged hydrocolloids or small molecular weight compounds to form complexes. These complexes could potentially be used for mouth-feel improvement in food industry (Carvalho et al., 2006) and drug delivery in pharmaceutical industry (Weinbreck, Tromp, & de Kruif, 2004). Gum arabic is a thickening agent commonly used in food product development, such as flavor encapsulation. Espinosa-Andrews et al. (2007) investigated the interactions between gum arabic and chitosan by examining the influence of gum arabic/chitosan ratio, total polymer concentration, pH and ionic strength upon the electrostatic complexes formation. Their turbidity and electrophoretic mobility results showed that the optimized gum arabic/chitosan mass ratio was 5 for coacervate formation. The maximized gum arabic–chitosan interaction could be obtained within the pH range between 3.5 and 5 (Espinosa-Andrews et al., 2007). Another negatively charged compound worth noting is sodium tripolyphosphate (TPP), a small molecular weight crosslinker carrying five negative charges in each molecule. TPP has been approved as a GRAS ("generally recognized as safe") reagent by FDA. Chitosan (CS) and TPP can form nanoparticles through electrostatic interaction, which has previously been investigated for different delivery applications (Gan & Wang, 2007; Hu et al., 2008; Jang & Lee, 2008; Ko, Park, Hwang, Park, & Lee, 2002; Wu et al., 2005). One interesting formulation among them is CS–TPP nanoparticles developed through an O/W emulsion route for entrapping hydrophobic felodipine (Ko et al., 2002). After felodipine was entrapped into CS–TPP nanoparticles, the control release of felodipine could be achieved by tuning pH, initial concentration, and molecular weight during nanoparticles preparation.

Previous studies suggest that CS–TPP nanoparticles are very useful carriers for drug and nutraceutical delivery. It is known that the CS–TPP particles were formed mainly through the electrostatic interaction between positively charged chitosan and negatively charged TPP molecules. However, how the CS–TPP particle sizes affect their packing, as well as the rheological properties of the resulted complex fluids (either chitosan–TPP particle suspensions or microgels) have been scarcely reported. In this paper, chitosan particles of different sizes were prepared through the use of TPP and ultrasonication. Depending on particle sizes, either CS–TPP particle suspensions or microgels were obtained after centrifugation at 11,000 × *g*, and their corresponding rheological properties were investigated by both static and dynamic rheological measurements. The static rheological technique measured the apparent viscosity (η) of polymer solution as a function of shear rate, while dynamic frequency test determined the storage modulus (G') and loss modulus (G'') as a function of angular frequency (ω). The correlation between particle sizes and particle packing profiles was also explored through rheological measurements.

2. Materials and methods

2.1. Materials

Chitosan with deacetylation degree (DD) of 98.0% and molecular weight (M_w) of 330 kDa was purchased from Kunpoong Bio. Co., Ltd. (South Korea). Sodium tripolyphosphate (TPP, 85%, technical grade) was purchased from Acros Organics (Morris Plains, NJ). Acetic acid, glacial (ACS grade) was purchased from Fisher Scientific (Fair Lawn, NJ). All of these reagents were used as received. Milli-Q (18.3 MΩ) water was used in all experiments.

2.2. Methods

2.2.1. Preparation of chitosan–sodium tripolyphosphate (CS–TPP) nanoparticles

Different amounts of chitosan (CS, 330 kDa) were dissolved in 2 wt% acetic acid solution to form chitosan solutions with concentrations ranging from 1 mg/mL to 30 mg/mL. Sodium tripolyphosphate (TPP) was dissolved in Milli-Q water to form a 200 mg/mL solution. CS–TPP nanoparticles were formed by dropwise addition of TPP solution into chitosan stock solution at different CS/TPP mass ratios under severe magnetic stirring. The change of solution volume caused by the addition of TPP solution was negligible due to the large CS/TPP volume ratio. After vortexing for 5 min, 40 mL of each CS–TPP particle suspension was processed under ultrasonication (Sonifier Cell Disruptor, Model W-350, Branson Sonic Power Co.) with 3.75 W/mL energy output and the duration varying from 3 to 9 min to obtain chitosan particles with controlled particle sizes. High speed centrifugation at ambient condition was set at 11,000 × *g* for 50 min to separate the microgel and supernatant. The supernatant was then removed, and the remaining microgels were washed with 2 wt% acetic acid buffer for three times prior to the rheological study.

2.2.2. Particle size measurements

Photon correlation spectroscopy (PCS)-based BIC 90 plus particle size analyzer equipped with a Brookhaven BI-9000AT digital correlator (Brookhaven Instrument Corporation, New York, USA) was used to measure hydrodynamic diameters (d) and size distribution of CS–TPP nanoparticles. The light source is a solid state laser operating at the wavelength of 658 nm with 30 mW power, and the signals were detected by a high sensitivity avalanche photodiode detector. All measurements were conducted at 25 ± 1 °C with the detection angle of 90°. CS–TPP nanoparticle suspensions were diluted with buffer until their viscosities were close to that of water (i.e., 0.89 cp at 25 °C). The normalized field–field autocorrelation functions $g(q,t)$ were obtained from the intensity–intensity autocorrelation functions, $G(q,t)$, via the Sigert relation (Stepanek, 1993). Both single stretched exponential fit and Cumulant analysis method were used in our particle size measurements (Wang et al., 2008).

2.2.3. Rheological measurements

Rheological measurements of the CS–TPP nanoparticle suspensions were performed by using ARES Rheometer (Rheometrics Scientific, NJ) with either cone and plate geometry (diameter 50 mm, cone angle 4°) or parallel plate geometry (diameter 25 mm) at ambient temperature (approximately 25 °C). Steady sweep measurements were carried out by applying shear rate from 1 to 1000 s^{-1} with 20 data points per decade. Zero shear viscosities, the viscosities at vanishing shear rates, were determined by extrapolating the Newtonian plateau to zero shear rate. Prior to a dynamic frequency sweep test, dynamic strain sweep test ranging from 0 to 100% was performed at 2 rad/s angular frequency. In this paper, the strain was fixed at 0.5% and the angular frequency ω was ranged

Table 1
Physical states of sodium tripolyphosphate (TPP)-crosslinked chitosan (CS) particles at different initial CS and TPP concentrations.

	TPP0.1 mg/mL	TPP0.5 mg/mL	TPP1.0 mg/mL	TPP1.5 mg/mL	TPP2.0 mg/mL
CS 1.0 mg/mL	○	○	◊	□	□
CS 1.5 mg/mL	○	○	◊	◊	□
CS 2.0 mg/mL	○	○	◊	◊	◊

○: transparent; ◊: suspension; □: precipitation.

from 0.1 to 100 rad/s. Small amount of mineral oil was utilized to seal the sample edge to prevent solvent evaporation. The gap between one plate or cone and the other plate was properly selected to avoid sample slip.

2.2.4. Atomic force microscopy (AFM) measurements

Images of CS–TPP nanoparticles were collected by a commercial Nanoscope IIIa Multi-Mode AFM (Veeco Instruments, CA) equipped with a J scanner, which was operated in tapping mode using silicon cantilever. The scanned images were obtained at the scan size of 2.0 μm × 2.0 μm and the scan frequency of 0.75 Hz. The CS–TPP nanoparticle suspensions for AFM imaging were prepared by solution immersion on silicon wafers. Those silicon wafers were immersed in the CS–TPP nanoparticle suspension for 1 h, washed by Milli-Q water and dried by nitrogen gas prior to morphological measurements.

2.2.5. Attenuated total reflection Fourier transformed infrared spectroscopy (ATR-FTIR)

The ATR-FTIR spectra were collected at ambient temperature using a Thermo Nicolet 670 FT-IR Spectrometer (Thermo Electron Corp, Madison, WI) with a Smart MIRacle horizontal attenuated total reflectance Ge crystal accessory. Each spectrum was averaged over 512 scans with 4 cm^{-1} resolution in the wavenumber range of 600–4000 cm^{-1}.

2.2.6. Water content measurement

The water contents of the CS–TPP microgels were determined by dry-weighing method. The CS–TPP microgel samples were weighed before and after fully drying by a balance with four digits after decimal point. The weighing process was duplicated for three times.

2.2.7. Theory for particle–particle interaction

The stabilization of CS–TPP nanoparticle suspensions or microgels depends upon particle–particle interaction which involves electrostatic repulsion and van der Waals attraction. For suspensions, electrostatic interaction between positively charged CS–TPP nanoparticles maintained particle stability. For microgels, the collective effect of van der Waals force and electrostatic interaction played a dominant role in the microgel formation. To qualitatively understand the effect of particle sizes on the rheological properties of microgels, Lennard–Jones potential was applied to determine van der Waals interaction between a pair of CS–TPP particles while Debye–Hückle theory was adopted here for the electrostatic potential (Li, Lee, Lal, An, & Huang, 2008). For van der Waals potential, the Lennard–Jones equation was shown as follows:

$$U_{vdw}\ (r) = U_{0v}\left[\left(\frac{r_0}{r}\right)^{12} - 2\left(\frac{r_0}{r}\right)^{6}\right] \quad (1)$$

where r_0 was the van der Waals radii of CS–TPP particle, r was the particle–particle interaction range, and U_{0v} was the depth of the interaction well.

For electrostatic potential, the Debye–Hückle equation was displayed as follows:

$$U_{ele}\ (r) = \frac{\Delta S^2 \rho_1 \rho_2}{4\pi\varepsilon r} e^{r/\lambda_D} \quad (2)$$

where r is the particle–particle interaction range; ε, which equaled 0.18 e^2/pN nm^2 at room temperature in water, was the dielectric constant of 2% (v/v) acetic acid buffer; ρ_1 and ρ_2 were the surface charge densities of CS–TPP nanoparticle 1 and nanoparticle 2; ΔS was the projection area of a CS–TPP nanoparticle; λ_D, which was approximately equal to $0.304\varphi^{-1/2}$ (nm) for monovalent salts, where φ (mol/L) was the monovalent salt concentration, was the Debye screening length (Niebuhr & Koch, 2005). The above two equations combined were used to obtain the total potential of CS–TPP particles in the microgel state.

3. Results

3.1. Morphology and sizes of CS–TPP nanoparticles

Fig. 1A displays the tapping mode AFM height image of CS–TPP nanoparticles in dry state on the silicon wafer, which indicates the pseudo-spherical morphology of CS–TPP nanoparticles. Some particles were overlapped with each other. Section analysis embedded in the software Nanoscope5.30 was applied to calculate the particle size on the wafer surface. The vertical distance from the upper edge of the particle to the bottom of the silicon wafer was taken as particle size, which was previously utilized to calculate size of oat protein isolate in dry state (Liu et al., 2009). The individual particle sizes of those CS–TPP nanoparticles (prepared at initial chitosan concentration of 1.5 mg/mL) from section analysis are approximately 20–30 nm. Fig. 1B and C shows the autocorrelation function curve of dynamic light scattering (DLS) and its corresponding size distribution, respectively. The minimum particle size calculated from curve fitting through Stocks–Einstein's equation turns out to be 170 nm. The particle sizes calculated from AFM were smaller than those from DLS, which was mainly due to difference in sample states. AFM gave the particle images in dry state while DLS provided average particle size in solution. The particle size calculated from DLS contained hydrated layers surrounding the nanoparticles which disappeared for dried nanoparticles in AFM measurement. Besides, the existence of CS–TPP particle aggregates also contributed to the larger DLS value. Similarly, Wu et al. (2005) found that the sizes of chitosan nanoparticles (20–80 nm) determined by TEM were smaller than those determined by DLS (>120 nm) in water.

3.2. Effect of CS/TPP mass ratio

Table 1 shows the physical states of CS–TPP complexes at different initial TPP and CS concentrations. At low TPP concentrations (i.e., lower than 0.5 mg/mL), the amount of TPP was not enough to fully crosslink chitosan chains, and the solutions remained transparent. Further increase of TPP concentration (i.e., higher than 1 mg/mL) led to an increase in particle sizes, resulting in either suspension or precipitation. Fig. 2 shows the hydrodynamic diameters of CS–TPP complexes under different CS and TPP concentrations. Chitosan concentrations between 1 mg/mL and 2 mg/mL were chosen because higher concentrations (i.e., 10 mg/mL chitosan solution) could significantly alter the rheological properties of CS–TPP complexes. The formation of CS–TPP nanoparticles mainly depends upon CS/TPP mass ratio when chitosan concentration is

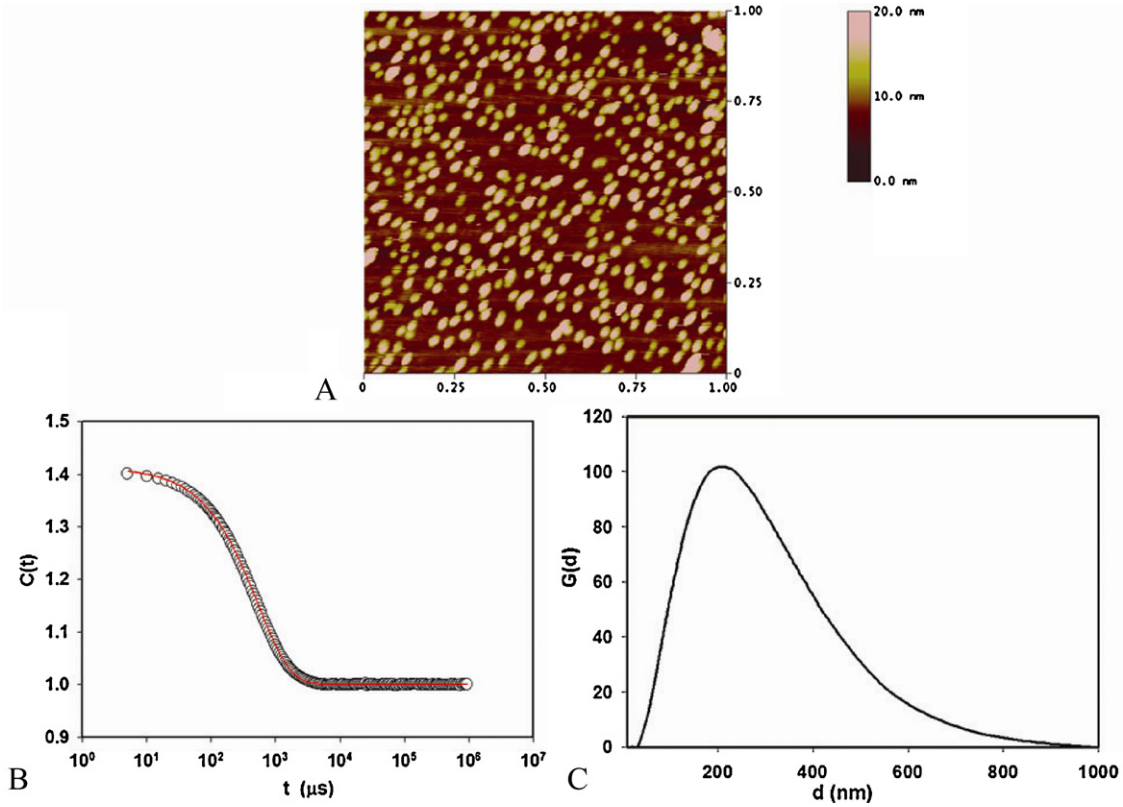

Fig. 1. Typical tapping mode-atomic force microscopy (AFM) height image (A), dynamic light scattering autocorrelation function and its fitting curve (B), as well as its particle size distribution obtained from Cumulant analysis (C) for chitosan–sodium tripolyphosphate (CS–TPP) particles prepared at initial CS/TPP mass ratio of 3.75. The chitosan concentration was fixed at 1.5 mg/mL and the AFM scan size is 1 μm × 1 μm.

relatively low. The optimum CS/TPP mass ratio condition at low chitosan concentration could also be determined, and Fig. 2 shows that the optimum CS/TPP mass ratio for the minimum particle sizes is 3.75, which is in agreement with previous results (Hu et al., 2008; Jang & Lee, 2008; Wu et al., 2005). To obtain chitosan particles of different sizes, ultrasonication (energy output of 3.75 W/mL) was also used as a complementary tool to break down the particle aggregates. Previously, Wu et al. reported that low chitosan concentration could increase the drug encapsulation capability. They recommended that for 1 mg/mL TPP crosslinker solution, chitosan concentration should be kept within the range of 0.5–4 mg/mL (Wu et al., 2005). Jang and Lee (2008) suggested that low molecular weight chitosan and TPP formed nanoparticles of minimum sizes at the CS/TPP mass ratio of 2.5. Combining the results of zeta-potential with dynamic light scattering, Hu et al. (2008) concluded that the optimized CS/TPP mass ratio was 5. In this paper, the CS/TPP mass ratio of 3.75 was used in our following AFM, FTIR, and rheological experiments.

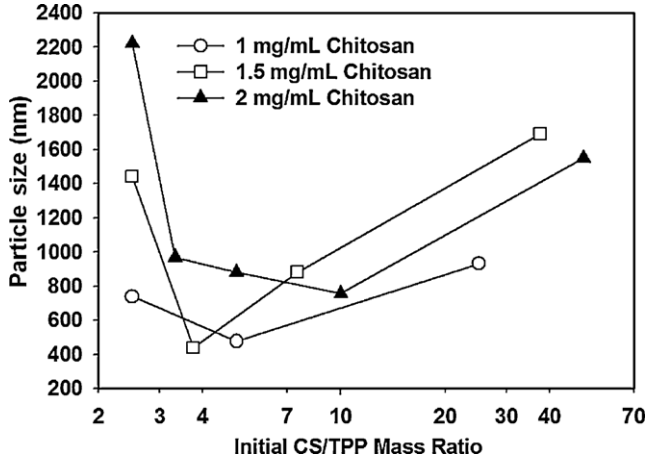

Fig. 2. Effect of initial chitosan/sodium tripolyphosphate (CS/TPP) mass ratios upon particle sizes of CS–TPP particles under different initial chitosan concentrations: 1 mg/mL (empty circles); 1.5 mg/mL (empty square); and 2 mg/mL (solid triangles).

3.3. FTIR analysis of CS–TPP nanoparticles

Fig. 3 shows the ATR-FTIR spectra of (A) pure chitosan (CS), (B) CS–TPP nanoparticle, and (C) pure TPP in the wavenumber range of 4000–600 cm^{-1}. For pure chitosan (Fig. 3A), the characteristic bands due to the stretching vibration of $-NH_2$ and –OH groups were observed at 3356 cm^{-1}. The feature peak at 1547 cm^{-1} for amide II (N–H bending vibration) and the small shoulder peak at 1647 cm^{-1} for amide I (–CO stretching vibration) indicate the high degree of deacetylation of chitosan. The flattening of the amine peak at 3356 cm^{-1} in Fig. 3B indicates that majority of amino group of chitosan participated in the electrostatic interaction with TPP. The characteristic peak located at 1206 cm^{-1} is assigned to P=O groups of TPP (Fig. 3C). The disappearance of that peak in the IR spectra of CS/TPP particle is another evidence of electrostatic interaction between the negatively charged phosphate group in TPP and positively charged amino group in chitosan.

3.4. Rheological properties

Fig. 4A displays the plot of apparent viscosities versus shear rate for chitosan (CS) solutions and corresponding CS–TPP particle suspensions of three different initial chitosan concentrations (i.e., 15 mg/mL, 10 mg/mL, and 8 mg/mL). All of the CS

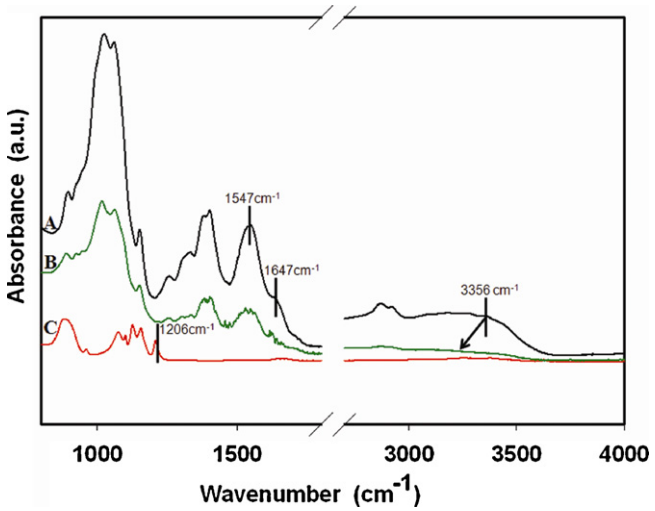

Fig. 3. FTIR spectra of (A) pure chitosan powder (M_w = 330 kDa, degree of deacetylation = 98%), (B) chitosan–sodium tripolyphosphate (CS–TPP) particle prepared at initial CS/TPP mass ratio of 3.75 under 4 min sonication with 3.75 W/mL energy input (the initial chitosan concentration was 10 mg/mL), and (C) sodium tripolyphosphate powder.

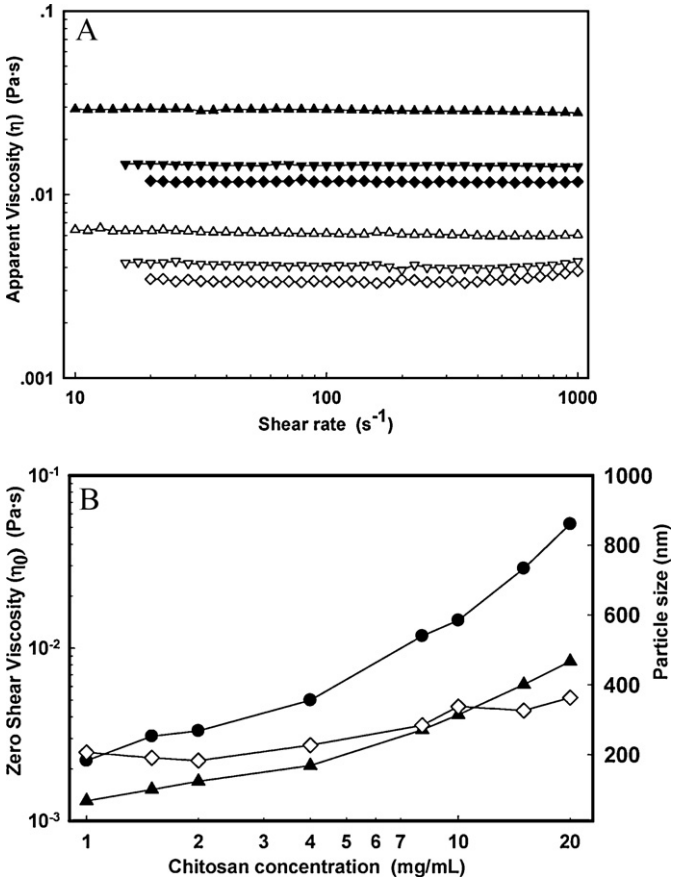

Fig. 4. (A) The curves of apparent viscosity versus shear rate for chitosan (CS) solutions and CS–TPP particle suspensions: (▲) 15 mg/mL chitosan solution; (▼) 10 mg/mL chitosan solution; (♦) 8 mg/mL chitosan solution; (△) 15 mg/mL CS–TPP suspension; (▽) 10 mg/mL CS–TPP suspension; (◊) 8 mg/mL CS–TPP suspension and (B) the plot of zero shear viscosity as a function of chitosan concentration for (•) pure chitosan solution, (▲) CS–TPP nanoparticle suspension, and the plot of particle size as a function of chitosan concentration for (◊) CS–TPP suspensions.

solutions and CS–TPP suspensions exhibited Newtonian flow behavior. The apparent viscosities of 8 mg/mL, 10 mg/mL, and 15 mg/mL chitosan (CS) solutions were 0.012 Pa s, 0.015 Pa s, and 0.029 Pa s, respectively. In contrast, the apparent viscosities of 8 mg/mL, 10 mg/mL, and 15 mg/mL CS–TPP particle suspensions decreased to 0.003 Pa s, 0.004 Pa s, and 0.006 Pa s, respectively. Chitosan chains carried positive charges at pH below 6.4 while TPP was negatively charged from pH 2 to pH 6.4. The formation of compact chitosan particles reduced the affinity of chitosan molecules with water, leading to the reduced viscosities.

Fig. 4B shows the plot of zero shear viscosities versus initial chitosan concentrations for CS solutions and CS–TPP suspensions (partially obtained from Fig. 4A). The particle sizes of CS–TPP particles ranged from 180 nm to 360 nm. One notes that the increase of initial chitosan concentration results in bigger particle sizes. Similar results were also reported by Hu et al. (2008), who showed that the particle size increased linearly with the increase of chitosan concentration. The lower dependency of the apparent viscosities of TPP-crosslinked chitosan nanoparticles on the initial chitosan concentration is probably due to the compact nature of chitosan nanoparticles.

Fig. 5A shows the applied strain dependence for storage modulus (G') and loss modulus (G'') at the angular frequency of 2 rad/s. CS–TPP microgels, which were prepared through the centrifugation of chitosan sub-micrometer particles, displayed strain-softening behavior which was also found in chitosan-modified nanoclay at highly hydrated state (Liang, Liu, Huang, & Yam, 2009). Here, the strain was fixed at 0.5% for dynamic oscillatory shear analysis, which was within the linear viscoelastic region. In Fig. 5B, G' of all the microgels consistently showed higher values than G'' over the frequency range studied (i.e., 0.1–100 rad/s), suggesting the elastic behavior for these CS–TPP complexes. And the large difference between G' and G'' indicates a strong microgel. As oscillatory frequency increased, the G' slightly increased before reaching a plateau at high frequency region. In contrast, the G'' increased to a larger degree as with the increase of frequency, suggesting that a high oscillatory shear may weaken the original microgel structure and turn a tight gel into a loose structure.

The plots of G' and G'' as a function of particle sizes at ω = 1 rad/s and shear strain = 0.5% are presented in Fig. 5C. One notes that G' is always larger than G'' over the entire particle size range (i.e., 336–868 nm), indicating gel-like structure of CS–TPP microgels. There were two regions in Fig. 5C: In the first particle size region (336–546 nm), G' increased significantly from 1000 Pa (particle size of 336 nm) to 10,568 Pa (particle size of 546 nm); further increase of particle sizes from 546 nm to 868 nm led to a smaller increase in G', which reached an ultimate value of 20,404 Pa. This phenomenon illustrates that larger particles tend to form stronger microgels.

3.5. Water content of CS–TPP microgels

In order to further analyze the composition of CS–TPP microgels, the water content within the microgels was determined by weight-loss analysis technique. Fig. 6 exhibits the water content of CS–TPP microgels prepared from CS–TPP complexes of different particle sizes. All CS–TPP microgels had a water content of about 87%. No obvious change in the water content with the sizes of the CS–TPP particles was observed. We interpret this as due to the relatively homogeneous packaging of CS–TPP particles, in which each particle behaved like a hard sphere, and its free volume (interspace between particles) depended upon the packing pattern rather than the particle sizes.

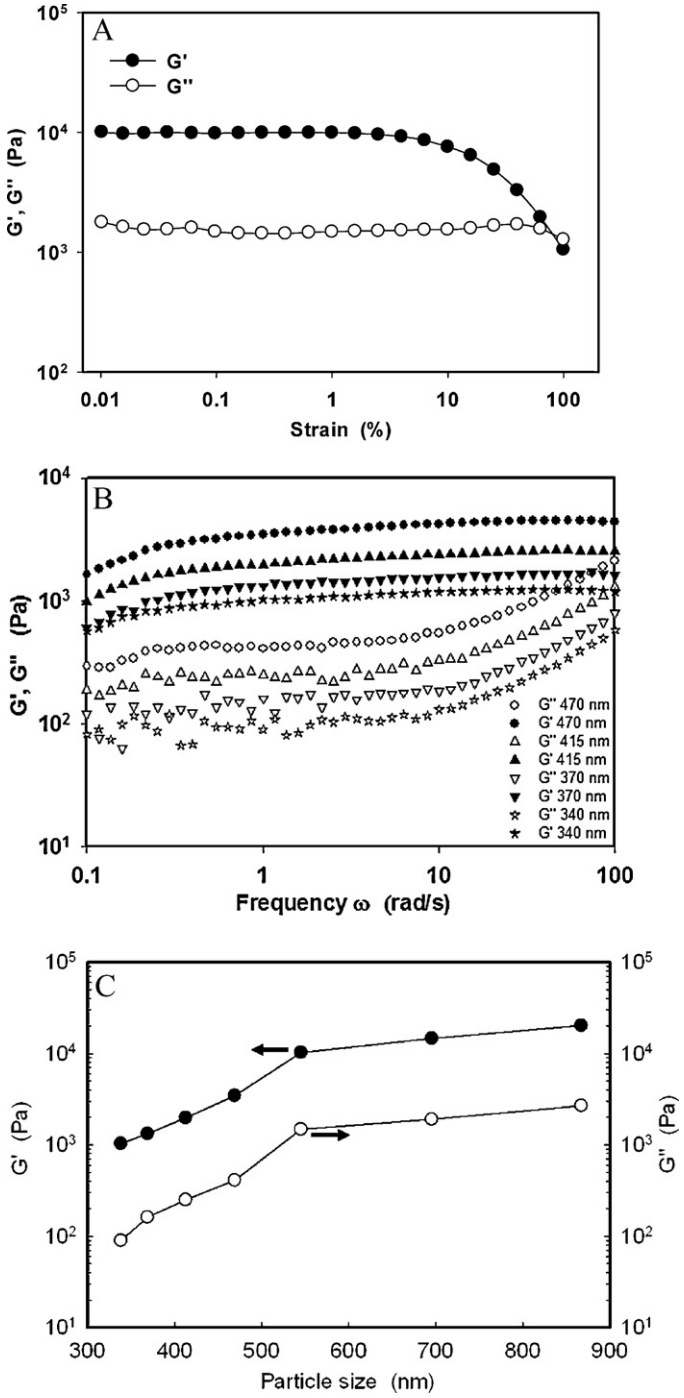

Fig. 5. (A) Storage modulus (G') and loss modulus (G'') as a function of strain (%) for chitosan–sodium tripolyphosphate (CS–TPP) microgels prepared at initial chitosan concentration of 20 mg/mL under 6 min sonication with 3.75 W/mL energy input [•: storage modulus (G') and ○: loss modulus (G'')]. (B) Storage modulus (G', filled) and loss modulus (G'', empty) as a function of angular frequency (ω) at strain = 0.5% for CS–TPP microgels prepared with different particle sizes (circles, 470 nm; up triangles, 415 nm; down triangles, 370 nm; and stars, 340 nm). (C) Effect of particle sizes on the storage modulus (G') and loss modulus (G'') of CS–TPP microgels [•: storage modulus (G'') and ○: loss modulus (G'')]. Here angular frequency (ω) and strain were fixed at 1 rad/s and 0.5%, respectively.

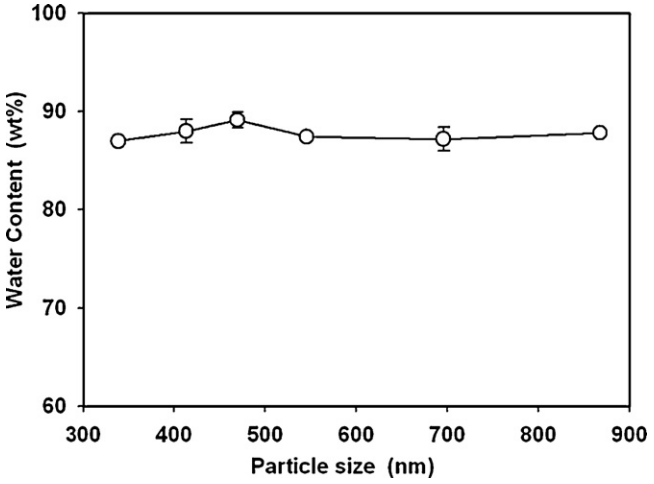

Fig. 6. The plot of water contents of chitosan–sodium tripolyphosphate (CS–TPP) microgels versus particle sizes.

4. Discussion

Chitosan formed complexes/particles after being crosslinked by TPP. Calvo's classical procedure was commonly adopted by many researchers to directly prepare CS–TPP nanoparticles (Calvo, RemunanLopez, VilaJato, & Alonso, 1997a; Calvo, RemunanLopez, VilaJato, & Alonso, 1997b). Due to electrostatic interaction between chitosan and TPP, many physicochemical factors, including pH, ionic strength, CS/TPP mass ratio, initial chitosan concentration and processing methods can affect the stability of CS–TPP particle suspensions. Here we optimized the condition for CS–TPP nanoparticle formation by varying CS/TPP mass ratio, chitosan concentration, and ultrasonication conditions prior to rheological measurement. The CS/TPP mass ratio affected TPP's crosslinking efficiency, while the chitosan concentration influenced fluid viscosity, particle–particle distance, and surface charges of the particles directly. It was also reported that chitosan concentration could affect the zeta-potential of CS–TPP nanoparticles. Higher chitosan concentration caused more unneutralized $-NH_3^+$ on the surface of nanoparticles, which further led to much stronger electrostatic repulsion between particles (Hu et al., 2008). Unlike the conventional CS–TPP complex formulation, ultrasound processing used in the current research further decreased the particle size by breaking down the aggregates, and simultaneously enhanced their storage stability. In addition to our variables for optimization, the effect of chitosan molecular weight on particle size could not be ignored either. Janes et al. confirmed that chitosan of lower molecular weight tended to form smaller nanoparticles because shorter chitosan chains were easier to penetrate into the CS–TPP complexes, resulting in a denser pattern. CS/TPP mass ratio, one of the most important processing parameters, was optimized without sonication so that we could determine the crosslinking efficiency under natural condition. After fixing the CS/TPP mass ratio, both chitosan concentration and sonication time were selected as adjustable parameters to control the particle sizes of CS–TPP nanoparticles during rheological measurement.

At the concentration range studied, both chitosan solutions and CS–TPP nanoparticle suspensions show Newtonian flow behavior within the major shear rate range, which is good for scale-up processing. Compared with chitosan solutions, CS–TPP nanoparticle suspensions were of much lower viscosity at the same chitosan concentration. This is because TPP-crosslinked chitosan molecules turned into more dense particles whose hydrodynamic volumes were smaller than pure chitosan chains. Fewer free chitosan chains and more crosslinked chains result in a decrease of total hydrodynamic volumes of chitosan. When the total hydrodynamic volume of chitosan is smaller than the solution volume, chitosan chains do not entangle with each other.

For CS–TPP microgels prepared from centrifugation of CS–TPP particle suspensions with initial particle sizes larger than 300 nm,

two regions of G' and G'' were observed, as shown in Fig. 5C. Here, different particle sizes were achieved by adjusting initial chitosan concentration and sonication time. The microgels with particle sizes ranging from 340 nm to 470 nm were prepared from 10 mg/mL chitosan solution, while the rest of the microgels were prepared from chitosan solution of higher concentration (i.e., 20 mg/mL). In the first region, the ultrasonication processing time was utilized to tune the particle size. Compared with sonication time, chitosan concentration exhibited a higher impact upon the storage and loss modulus, hence the particle packing density of CS–TPP microgels. At the same chitosan concentration, elastic modulus and loss modulus maintained a linear increase relationship on the semi-log scale with sonication period. The particle sizes of CS–TPP microgels ranging from 340 nm to 870 nm were suitable for high speed centrifugation. Consistently larger G' than G'' over the entire frequency range studied suggested the elastic behavior of CS–TPP microgels, as shown in Fig. 5B. The impact of particle sizes on the rheological properties of CS–TPP microgels may be related to the difference in particle packing profiles within the microgels. The higher G' of CS–TPP microgels at larger particle sizes indicated that larger particles tended to form tighter particle packing in microgels. The centrifugal force had a bigger influence on large particles than small particles, resulting in higher particle packing density and stronger interparticle interactions within the microgels.

For TPP-crosslinked chitosan particle suspension, electrostatic interaction plays an important role in preventing particle aggregation which can be verified by high value of CS–TPP nanoparticles' zeta-potential (averaged ~65 mV). For chitosan-based gels, the stabilization of gel structure is complicated. Different gel formations result from different gelation mechanisms. By proper manipulation, pH-induced chitosan hydrogel can be achieved. Ta, Han, Larson, Dass, and Dunstan (2009) prepared a thermo sensitive orthophosphate–chitosan hydrogel which can be used for drug delivery. They prepared the gel by mixing dipotassium hydrogen orthophosphate and chitosan solutions at low temperature and obtained the gel through elevating temperature. Similar protocol has also been adopted by Chenite et al. for β-glycerol phosphate/chitosan hydrogel preparation (Chenite et al., 2000; Chenite, Buschmann, Wang, Chaput, & Kandani, 2001). The preparation involved a sol–gel transition, and several interactions, including hydrogen bonding, electrostatic attraction and hydrophobic interaction are responsible for this transition. In their systems, the addition of glycerol phosphate can increase pH while prevent precipitation of chitosan through electrostatic interaction, and promote gel formation upon elevating temperature through enhancing hydrophobic interactions among chitosan chains. The increase of temperature strengthened the dehydration of chitosan chains by glycerol moiety, hence the hydrophobic interaction among chitosans, which led to the formation of homogeneous gel. Thus, for chitosan–phosphate system, hydrophobic interaction plays a major role in the gelation while hydrogen bonding and electrostatic interaction also helps the gel formation. However, in our CS–TPP microgel system, the high speed centrifugation provides driving force to settle down CS–TPP particles in a crowded packing manner. The large centrifugal force (11,000 × g for CS–TPP microgels) can overcome the barrier of electrostatic repulsion between CS–TPP particles in suspension and stick them together. The centrifugal force provides strong interfacial tension (γ) between CS–TPP particles. Considering the basic Newton Force Law, the relationship between interfacial tension (γ) and the radius of particle (r) is established as follows:

$$\gamma = \frac{F_{cen}}{S} \sim \frac{ma}{4f\pi r^2} \sim r \quad (3)$$

where F_{cen} is the centrifugal force acting on particles, S is the interfacial area between particles, m is particle mass, a is the centrifugal acceleration of the particle, f is the fraction of surface in-contact between particles and r is the particle radius. Fig. 7A displays the schematic diagram of interfacial tension between CS–TPP particles. Under the same centrifugal field, the interfacial tension between large particles tends to be larger than that between small particles. Higher interfacial tension (γ) between large particles results in a tighter particle packing, which is in agreement with the occurrence of large storage modulus (G') for microgels of large particles.

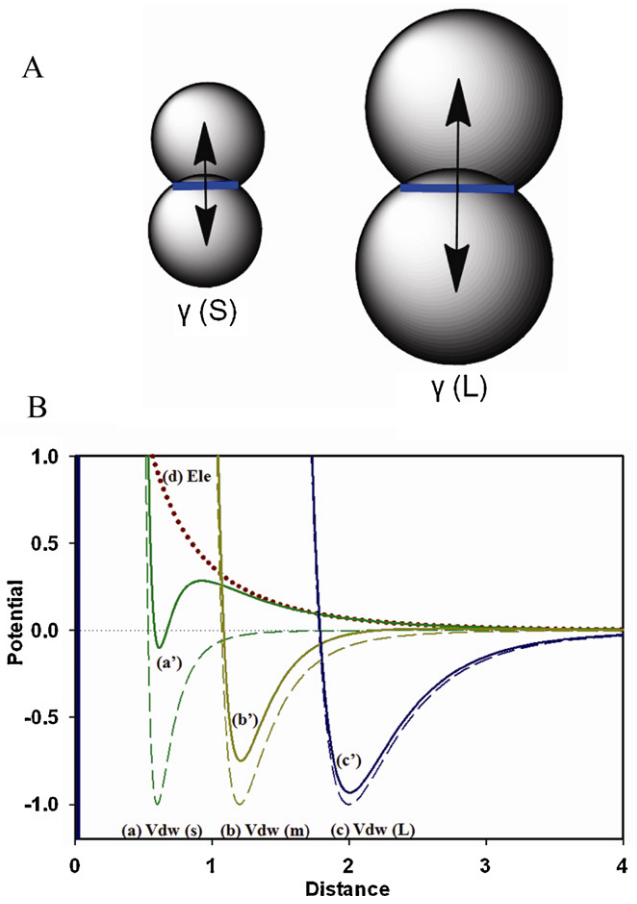

Fig. 7. (A) Schematic diagrams of interfacial tension (γ) between CS–TPP particles with different sizes during centrifugation processing. (B) Inter-particle interaction potential profiles of chitosan–sodium tripolyphosphate (CS–TPP) microgels which include van der Waals potential for small-sized CS–TPP particles (a), medium-sized CS–TPP particles (b), and large-sized CS–TPP particles (c); as well as electrostatic potential (d), total potential of small-sized CS–TPP particles (a′), medium-sized CS–TPP particles (b′), and large-sized CS–TPP particles (c′).

After centrifugation, the CS–TPP microgels were stabilized through particle–particle interaction which involved electrostatic repulsion and van der Waals interaction. For the established CS–TPP microgel, we proposed the following mechanism to explain the effect of particle sizes on interparticle interactions, as shown in Fig. 7B, which displays the van der Waals potential and electrostatic potential of CS–TPP particles under different particle size conditions. Since the zeta-potentials of CS–TPP particles with different particle sizes showed negligible difference, the electrostatic interaction between CS–TPP particles was kept unchanged (d curve in Fig. 7B). In CS–TPP microgel, the short particle distance greatly increased the van der Waals force among particles. For large particles, the contour of van der Waals potential is close to that of total energy potential, indicating the dominant contribution of van der Waals force. This energy potential analysis was also in agreement with the results from dynamic oscillatory shear analysis. Large particles interacted much stronger with each other, leading to tighter particle packing in microgels. Finally, research relevant to the use

of scattering techniques (Higgins & Benoît, 1996) to illustrate the nature of microgels packaging (i.e., face-centered cubic or hexagonally close-packed structure) is still undergoing in our laboratory.

5. Conclusion

CS–TPP particles with controlled particle sizes have been successfully prepared through the electrostatic interaction between amino groups of chitosan and phosphate groups of sodium tripolyphosphate. Different techniques including dynamic light scattering, atomic force microscopy, rheology, and Fourier transformed infrared spectroscopy were applied to characterize the structure and rheological properties of CS–TPP particles. The CS/TPP mass ratio of 3.75 was found to be the optimum condition to achieve minimum particle sizes. Both chitosan concentration (10 mg/mL and 20 mg/mL) and sonication period (3–9 min, 3.75 W/mL energy output) were utilized to control the particle sizes of CS–TPP particles. Compared with pure chitosan solutions, the formation of CS–TPP particle suspensions decreased the solution viscosity. During centrifugation processing, strong centrifugal force overcame the barrier of electrostatic interaction between CS–TPP particles in suspension, after which CS–TPP microgels formed. Through the analysis of van der Waals attraction and electrostatic repulsion, and in combination with DLS and rheological measurements, we found that large CS–TPP particles tended to form tighter microgel than the small particles. Besides, water content analysis may suggest the pseudo-hard sphere nature of CS–TPP particles.

Acknowledgements

We thank Drs. Yunqi Li and Songmiao Liang for the insightful discussion. This work was supported by US Department of Agriculture National Research Initiative Program (#2009-35603-05071).

References

Calvo, P., RemunanLopez, C., VilaJato, J. L. & Alonso, M. J. (1997a). Chitosan and chitosan ethylene oxide propylene oxide block copolymer nanoparticles as novel carriers for proteins and vaccines. *Pharmaceutical Research*, *14*(10), 1431–1436.

Calvo, P., RemunanLopez, C., VilaJato, J. L. & Alonso, M. J. (1997b). Novel hydrophilic chitosan–polyethylene oxide nanoparticles as protein carriers. *Journal of Applied Polymer Science*, *63*(1), 125–132.

Carvalho, E., Mateus, N., Plet, B., Pianet, I., Dufourc, E. & De Freitas, V. (2006). Influence of wine pectic polysaccharides on the interactions between condensed tannins and salivary proteins. *Journal of Agricultural and Food Chemistry*, *54*(23), 8936–8944.

Chenite, A., Buschmann, M., Wang, D., Chaput, C. & Kandani, N. (2001). Rheological characterisation of thermogelling chitosan/glycerol-phosphate solutions. *Carbohydrate Polymers*, *46*(1), 39–47.

Chenite, A., Chaput, C., Wang, D., Combes, C., Buschmann, M. D., Hoemann, C. D., et al. (2000). Novel injectable neutral solutions of chitosan form biodegradable gels in situ. *Biomaterials*, *21*(21), 2155–2161.

Espinosa-Andrews, H., Baez-Gonzalez, J. G., Cruz-Sosa, F. & Vernon-Carter, E. J. (2007). Gum arabic–chitosan complex coacervation. *Biomacromolecules*, *8*(4), 1313–1318.

Gan, Q. & Wang, T. (2007). Chitosan nanoparticle as protein delivery carrier—Systematic examination of fabrication conditions for efficient loading and release. *Colloids and Surfaces B: Biointerfaces*, *59*(1), 24–34.

Han, E., Shan, D., Xue, H. G. & Cosnier, S. (2007). Hybrid material based on chitosan and layered double hydroxides: Characterization and application to the design of amperometric phenol biosensor. *Biomacromolecules*, *8*(3), 971–975.

Higgins, J. S. & Benoît, H. (1996). *Polymers and neutron scattering*. Oxford: Oxford University Press.

Hu, B., Pan, C. L., Sun, Y., Hou, Z. Y., Ye, H. & Zeng, X. X. (2008). Optimization of fabrication parameters to produce chitosan–tripolyphosphate nanoparticles for delivery of tea catechins. *Journal of Agricultural and Food Chemistry*, *56*(16), 7451–7458.

Huang, Y., Yu, H., Guo, L. & Huang, Q. (2010). Structure and self-assembly properties of a new chitosan-based amphiphile. *Journal of Physical Chemistry B*, *114*(23), 7719–7726.

Janes, K. A., Calvo, P. & Alonso, M. J. (2001). Polysaccharide colloidal particles as delivery systems for macromolecules. *Advanced Drug Delivery Reviews*, *47*(1), 83–97.

Jang, K. I. & Lee, H. G. (2008). Stability of chitosan nanoparticles for L-ascorbic acid during heat treatment in aqueous solution. *Journal of Agricultural and Food Chemistry*, *56*(6), 1936–1941.

Ko, J. A., Park, H. J., Hwang, S. J., Park, J. B. & Lee, J. S. (2002). Preparation and characterization of chitosan microparticles intended for controlled drug delivery. *International Journal of Pharmaceutics*, *249*(1–2), 165–174.

Li, Y., Lee, J., Lal, J., An, L. & Huang, Q. (2008). Effects of pH on the interactions and conformation of bovine serum albumin: Comparison between chemical force microscopy and small-angle neutron scattering. *Journal of Physical Chemistry B*, *112*(12), 3797–3806.

Liang, S. M., Liu, L. S., Huang, Q. R. & Yam, K. L. (2009). Unique rheological behavior of chitosan-modified nanoclay at highly hydrated state. *Journal of Physical Chemistry B*, *113*(17), 5823–5828.

Liu, C. G., Desai, K. G. H., Chen, X. G. & Park, H. J. (2005). Preparation and characterization of nanoparticles containing trypsin based on hydrophobically modified chitosan. *Journal of Agricultural and Food Chemistry*, *53*(5), 1728–1733.

Liu, G., Li, J., Shi, K., Wang, S., Chen, J. W., Liu, Y. & Huang, Q. R. (2009). Composition, secondary structure, and self-assembly of oat protein isolate. *Journal of Agricultural and Food Chemistry*, *57*(11), 4552–4558.

Luo, K., Yin, J. B., Song, Z. J., Cui, L., Cao, B. & Chen, X. S. (2008). Biodegradable interpolyelectrolyte complexes based on methoxy poly(ethylene glycol)-b-poly(alpha,L-glutamic acid) and chitosan. *Biomacromolecules*, *9*(10), 2653–2661.

Niebuhr, M. & Koch, M. H. J. (2005). Effects of urea and trimethylamine-N-oxide (TMAO) on the interactions of lysozyme in solution. *Biophysical Journal*, *89*(3), 1978–1983.

Pillai, O. & Panchagnula, R. (2001). Polymers in drug delivery. *Current Opinion in Chemical Biology*, *5*(4), 447–451.

Richardson, S. C. W., Kolbe, H. J. V. & Duncan, R. (1999). Potential of low molecular mass chitosan as a DNA delivery system: biocompatibility, body distribution and ability to complex and protect DNA. *International Journal of Pharmaceutics*, *178*(2), 231–243.

Skotak, M., Leonov, A. P., Larsen, G., Noriega, S. & Subramanian, A. (2008). Biocompatible and biodegradable ultrafine fibrillar scaffold materials for tissue engineering by facile grafting of L-lactide onto chitosan. *Biomacromolecules*, *9*(7), 1902–1908.

Sogias, I. A., Williams, A. C. & Khutoryanskiy, V. V. (2008). Why is chitosan mucoadhesive? *Biomacromolecules*, *9*(7), 1837–1842.

Stepanek, P. (1993). Data analysis in dynamic light scattering. In W. Brown (Ed.), *Dynamic Light Scattering: The Method and Some Applications* (pp. 177–241). Oxford: Oxford University Press.

Ta, H. T., Han, H., Larson, I., Dass, C. R. & Dunstan, D. E. (2009). Chitosan-dibasic orthophosphate hydrogel: A potential drug delivery system. *International Journal of Pharmaceutics*, *371*(1–2), 134–141.

Wang, X. Y., Jiang, Y., Wang, Y. W., Huang, M. T., Ho, C. T. & Huang, Q. R. (2008). Enhancing anti-inflammation activity of curcumin through O/W nanoemulsions. *Food Chemistry*, *108*(2), 419–424.

Weinbreck, F., Tromp, R. H. & de Kruif, C. G. (2004). Composition and structure of whey protein/gum arabic coacervates. *Biomacromolecules*, *5*(4), 1437–1445.

Wu, Y., Yang, W. L., Wang, C. C., Hu, J. H. & Fu, S. K. (2005). Chitosan nanoparticles as a novel delivery system for ammonium glycyrrhizinate. *International Journal of Pharmaceutics*, *295*(1–2), 235–245.

Yao, Z., Zhang, C., Ping, Q. N. & Yu, L. L. (2007). A series of novel chitosan derivatives: Synthesis, characterization and micellar solubilization of paclitaxel. *Carbohydrate Polymers*, *68*(4), 781–792.

Yi, H. M., Wu, L. Q., Bentley, W. E., Ghodssi, R., Rubloff, G. W., Culver, J. N., et al. (2005). Biofabrication with chitosan. *Biomacromolecules*, *6*(6), 2881–2894.

Zhang, H., Mardyani, S., Chan, W. C. W. & Kumacheva, E. (2006). Design of biocompatible chitosan microgels for targeted pH-mediated intracellular release of cancer therapeutics. *Biomacromolecules*, *7*(5), 1568–1572.

Zhang, M. G., Smith, A. & Gorski, W. (2004). Carbon nanotube–chitosan system for electrochemical sensing based on dehydrogenase enzymes. *Analytical Chemistry*, *76*(17), 5045–5050.

Zhang, Y. Z., Su, B., Ramakrishna, S. & Lim, C. T. (2008). Chitosan nanofibers from an easily electrospinnable UHMWPEO-doped chitosan solution system. *Biomacromolecules*, *9*(1), 136–141.